Chinese Chemical Letters 32 (2021) 1942–1946

Contents lists available at ScienceDirect

Chinese Chemical Letters

journal homepage: www.elsevier.com/locate/cclet

Communication

Stellate porous silica based surface-enhanced Raman scattering system for traceable gene delivery

Lei Liu[a,b,c], Xin Du[d,e,*]

[a] Chemical Pharmaceutical Research Center, Tasly Academy, Tasly Holding Group Co., Ltd., Tianjin 300410, China
[b] Jiangsu Tasly Diyi Pharmaceutical Co., Ltd., Huaian 223003, China
[c] School of Chemical Engineering, The University of Adelaide, Adelaide, SA 5005, Australia
[d] Beijing Key Laboratory for Bioengineering and Sensing Technology, Department of Chemistry & Biological Engineering, University of Science & Technology Beijing, Beijing 100083, China
[e] Suzhou Nachuangjia Environmental Technology Engineering Co., Ltd., Suzhou 215133, China

ARTICLE INFO

Article history:
Received 5 October 2020
Received in revised form 30 December 2020
Accepted 30 December 2020
Available online 5 January 2021

Keywords:
Stellate porous silica
Au nanoparticles
Surface-enhanced Raman scattering
SERS trace
Gene delivery

ABSTRACT

Numerous nanocarriers have been currently developed for intracellular delivery. The potential cytotoxicity of these very small inorganic nanocarriers has raised great consideration. Thus, it becomes of utmost importance to conduct the intracellular trace of nanocarriers. Among many analytical techniques, surface enhanced Raman scattering (SERS) method is one of the current state-of-the-art techniques for cell visualization and trace. In this work, a novel stellate porous silica based gene delivery system has been designed for SERS trace purpose. A stellate porous silica nanoparticle modified with many small Au nanoparticles is designed to replace common metallic SERS tags. The results show that the designed system not only could deliver siRNA into cells for therapy, but also could realize SERS trace with high sensitivity and non-invasive features. The constructed delivery system has considerable potential to trace the dynamic gene delivery in living cells.

As a large majority of drug and gene therapy is limited by serious side effects, which caused by lethal dose and the rapid resistances of cancer cells, nanoscale drug/gene delivery systems have been employed. They are designed to overcome limitations caused by poor solubility and stability, low dosage, *in vivo* degradation, short circulating, poor pharmacokinetic profiles, and lack of 'free' therapeutic cargos selectivity. Currently, numerous nanocarriers with smart design and constructive advantages have been developed for intracellular delivery [1–8]. Although these nanosystems have high stability for mechanical and thermal changes, high biocompatibility, efficacious fabrication cost and low toxicity, the potential cytotoxicity of these very small inorganic nanocarriers has raised great considerations [9–14]. The trace study has been established to investigate intracellular delivery performances of the delivery systems.

For intracellular trace and cell visualization, many different analytical techniques have been developed. Light microscopy, electron microscopy and atomic force microscopy are used for a higher resolution cell visualization and subcellular structure observation. However, due to the limitation of their working principles, these methods only can collect the image of sample surfaces. The inside sub-structures of cells cannot be observed without killing and sectioning cells. External fluorescent tags are used for specifically reporting the cell structures, and fluorescence microscopy has been introduced for chemically selective trace. Confocal laser scanning fluorescence microscopy is widely utilized for visualizing intracellular uptake. However, each fluorescence reporter can only be excited by one distinct-wavelength laser, which causes the simultaneous trace of different structures has great limitations [15]. The artificial fluorescence label cannot avoid altering the physic-chemical characteristics of the analyzed system, which might trigger destructive problems. Alarmingly, photo-bleaching of fluorophores and fluorescent noises of the cell background might also interrupt the intracellular trace of carrier and drug [16].

In order to circumvent these issues, vibrational microscopy like surface enhanced Raman scattering (SERS) technique has been introduced for non-destructive trace. Unlike fluorescence method has problems such as rapid photo-bleaching and the background interruptions, Raman reporter are more photo-stable, and the

* Corresponding author at: Beijing Key Laboratory for Bioengineering and Sensing Technology, Department of Chemistry & Biological Engineering, University of Science & Technology Beijing, Beijing 100083, China.
E-mail address: duxin@mail.ipc.ac.cn (X. Du).

https://doi.org/10.1016/j.cclet.2020.12.061
1001-8417/

fingerprint Raman signals are easier to separate from the auto-fluorescence background [17]. Thus, the high sensitive and high resolution SERS method is regarded as one of the current state-of-the-art techniques for cell visualization and trace. In general, SERS is realized by the combination of SERS tags and Raman reporters. When these two parts are in the close vicinity, the electromagnetic field strength can significantly increase, which results in the enhancement of the Raman signal [18]. The common SERS tags are metallic nanoparticles such as silver and gold. General applied structures are nanospheres, while other complex structures such as nanorods [19–23], nanoflowers [24–28], nanostars [29–31] and metallic composites [32] have also been reported recently. However, most metallic SERS tags are high cost due to pure noble metal, and have shortage of the ability of gene delivery due to non-porous structure.

Herein, as shown in Scheme 1, we designed and fabricated a composite nanocarrier as a novel SERS tag by modifying many small Au nanoparticles on stellate porous silica nanoparticle (Au-ST-SiO_2), followed by the adsorption of Raman reporter (4-mercaptobenzoic acid, 4-MBA) and the loading of small interfering RNA (siRNA). The special Au@silica structure can endow the delivery system with active SERS effect. When the 4-MBA-Au-ST-SiO_2@siRNA are delivered to cancer cells, endocytosis phenomena and endosome escape should occur and siRNA molecules can release to the cytoplasm to carry out their pharmacological and anti-cancer functions. When observed with confocal Raman laser scanning microscopy, human osteogenic sarcoma (KHOS) cells incubated with 4-MBA-Au-ST-SiO_2@siRNA show SERS mapping with very obvious red color.

Stellate porous silica (ST-SiO_2) was synthesized by a sol-gel synthesis procedure [33,34]. Scanning electron microscopy (SEM) images exhibit that ST-SiO_2 has an average particle size of 80−120 nm (Figs. S1a and b in Supporting information). After the removal of surfactant, the uniform morphology of ST-SiO_2 is clearly demonstrated as nanospheres with center-radial pores of 10−30 nm, as shown in SEM (Figs. S1c and d in Supporting information) and transmission electron microscopy (TEM) images (Figs. 1a and b). The size is further verified by dynamic light scattering (DLS) measurement (Table S1 in Supporting information). The average hydrodynamic size of ST-SiO_2 is 97.2 nm with an average zeta potential of −30.5 ± 0.7 mV. The NH_2-ST-SiO_2 nanospheres were synthesized by the reaction of (3-aminopropyl) triethoxysilane (APTES) with silanol (Si−OH) *via* post-grafting amino groups. The successful modification of aminopropyl group on ST-SiO_2 was approved by The DLS result of NH_2-ST-SiO_2 show they have an average hydrodynamic size of *ca.* 105.0 nm with an average zeta potential of 27.1 ± 1.2 mV (Table S1). From ST-SiO_2 to NH_2-ST-SiO_2, the zeta potential changes from negative to positive,

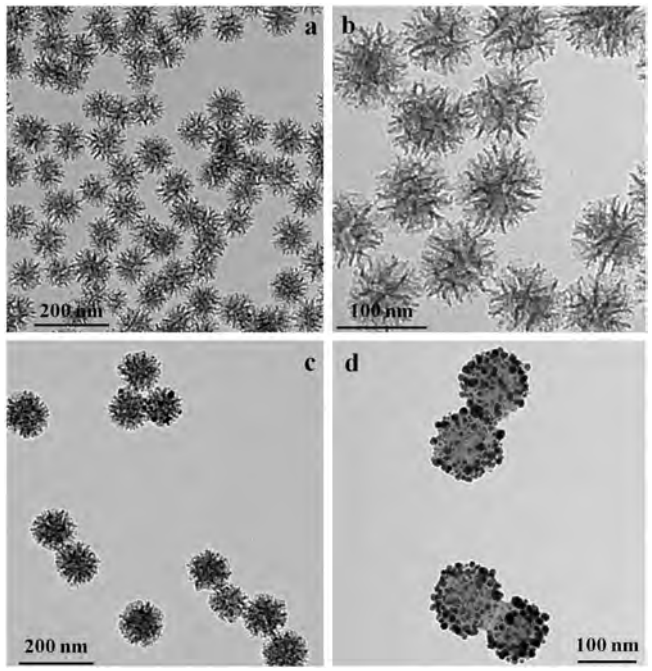

Fig. 1. TEM images of ST-SiO_2 (a, b) and Au-ST-SiO_2 (c, d) in low magnitude (a, c) and high magnitude (b, d).

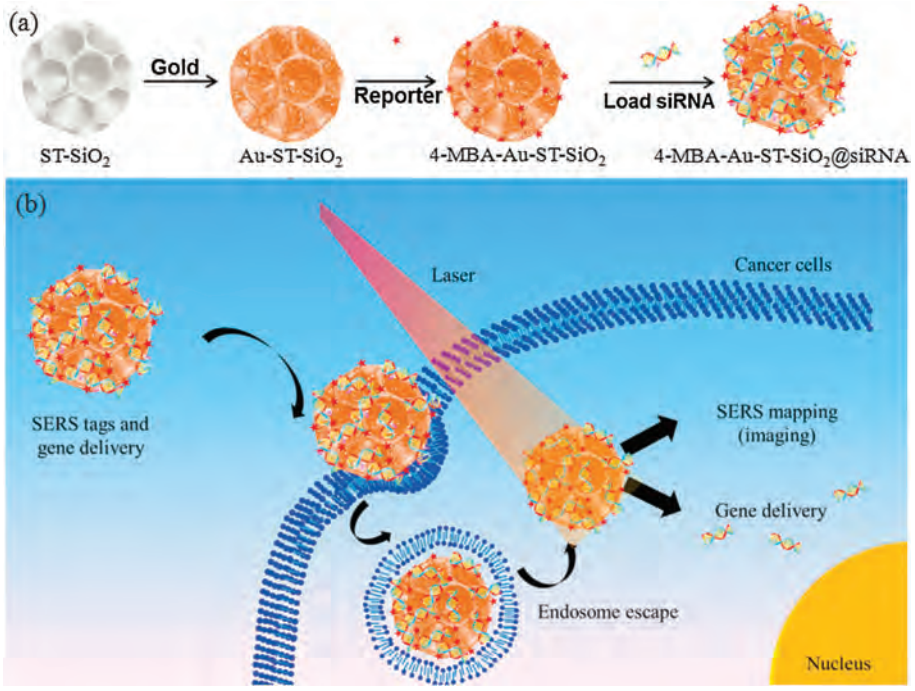

Scheme 1. (a) Fabrication of stellate porous silica based siRNA delivery system and (b) their possible intracellular siRNA delivery pathway and SERS traceable approach.

proving successful functionalization of amino groups. The surface modification of amino groups is important for anchoring Au nanoparticles *via* the strong coordination interaction between the empty d orbital of Au atom and the free pair of electrons on the N atom of the amino group [35]. Furthermore, Au-ST-SiO_2 was fabricated by *in-situ* reduction of $HAuCl_4{\cdot}3H_2O$ on NH_2-ST-SiO_2 *via* deposition-precipitation method [35]. As shown in TEM images (Figs. 1c and d), the prepared Au-ST-SiO_2 are uniform nanospheres with an average particle diameter around 100 nm. The aggregated Au nanoparticles are varied in size-range from 2 nm to 20 nm on the surfaces of NH_2-ST-SiO_2 skeletons. It can be noticed in Figs. 1c and d that small Au nanoparticles are distributed inside stellate pores and stable around NH_2-ST-SiO_2. From DLS (Table S1), Au-ST-SiO_2 composites have an average hydrodynamic size of 198.2 nm with zeta potential of 8.7 ± 0.6 mV. The large increase of particle size from 105.0 nm to 198.2 nm may be ascribed to two particle aggregation. The decrease of zeta potential value from ST-SiO_2-NH_2 to Au-ST-SiO_2 may be ascribed to the reduction of the exposed amino groups after the electrostatic adsorption between Au and amino groups. In addition, the capillary adsorption of stellate pores should be another contribution to the formation of Au@silica aggregation. Finally, 4-MBA-Au-ST-SiO_2 nanocarriers were fabricated by attaching Raman reporter 4-MBA on Au-ST-SiO_2 by the coordination interaction between -SH and gold [35,36]. From DLS (Table S1) and TEM images (Fig. S2 in Supporting information), these nanocarriers have an average hydrodynamic size of 202.1 nm with zeta potential of 7.9 ± 0.9 mV. Except a little decrease of zeta potential from 8.7 ± 0.6 mV to 7.9 ± 0.9 mV, no obvious difference in sizes or morphologies appears after 4-MBA combination because the percentage of the added 4-MBA in Au-ST-SiO_2 is quite low (0.1%).

X-ray diffraction (XRD) patterns and Fourier transform infrared (FT-IR) spectra were also employed to characterize these materials. From the wide-angle XRD pattern (Fig. 2a), the broad 2θ diffraction angle of 10 to 30° indicates the amorphous silica, while 2θ angles at 38.18°, 44.39°, 64.58° and 77.55° match the standard Au planes of (111), (200), (220) and (311) from JCPDS card. The intensity proportion of the tested sample can also match the standard one shown by red vertical line. In FT-IR spectra of ST-SiO_2 (Fig. 2b), peaks center at 1068 cm^{-1}, 945 cm^{-1} and 800 cm^{-1} can be attributed to the typical Si-O-Si asymmetric stretching, Si−OH and Si-O symmetric stretching vibrations. The peak centre at 1735 cm^{-1} is attributed to −COOH group vibration, proving the attaching of 4-MBA on Au-ST-SiO_2 (Fig. 2b). The 4-MBA attachment was also verified by Raman spectra (Fig. 2c). For pure Raman reporter 4-MBA, obvious Raman peaks at 1099.1 cm^{-1} and 1595.5 cm^{-1} are ascribed to υ8a and υ12 aromatic ring vibrations of 4-MBA [33]. However, in Raman spectrum of 4-MBA-Au-ST-SiO_2, the dominated peaks are centered at 1073.3 cm^{-1} and 1585.5 cm^{-1}. The blue shift is ascribed to the interaction between 4-MBA and Au nanoparticles.

Effective enhancement factor (EEF) of 4-MBA-Au-ST-SiO_2 can be roughly calculated by the eqution EEF = $I_{SERS}N_{bulk}/I_{bulk}N_{SERS}$ [36–38], where I_{SERS} and I_{bulk} are the intensities of SERS and bulk spectra at the 1078 cm^{-1}, and N_{bulk}/N_{SERS} is the molar ratio between the bulk and SERS sample. As shown in Fig. 2c, EEF of 4-MBA-Au-ST-SiO_2 is calculated as approximate 1.35×10^5, based on 1099.1 cm^{-1} of Raman peak and 1073.3 cm^{-1} of SERS peak. It means that the constructed 4-MBA-Au-ST-SiO_2 nanocarrier can indeed realize SERS phenomenon. The binding capability of siRNA on 4-MBA-Au-ST-SiO_2 nanocarriers was measured by agarose gel electrophoresis. For economic reason, instead of expensive siRNA, a model oligo DNA with same quantity of the bases was used in experiments. As shown in Fig. 2d, the weight ratio of nanocarriers to model DNA rangea from 10 to 200 with a naked oligo DNA as a control. The brightness of top binding DNA occurs and increases from weight ratio 50 to 200, showing the 4-MBA-Au-ST-SiO_2 nanocarrier has gene binding capability. In addition, the brightness decrease of escaped DNA also verifies gene binding.

The biocompatibility of 4-MBA-Au-ST-SiO_2 nanocarriers and the cytotoxicity of 4-MBA-Au-ST-SiO_2@siRNA were investigated by 3-(4,5-dimethylthiazol-2-yl)-2,5-diphenyltetrazolium bromide (MTT) assays against human embryonic kidney (HEK 293T) and KHOS cell lines. As illustrated in Fig. 3a, cell viabilities of both HEK

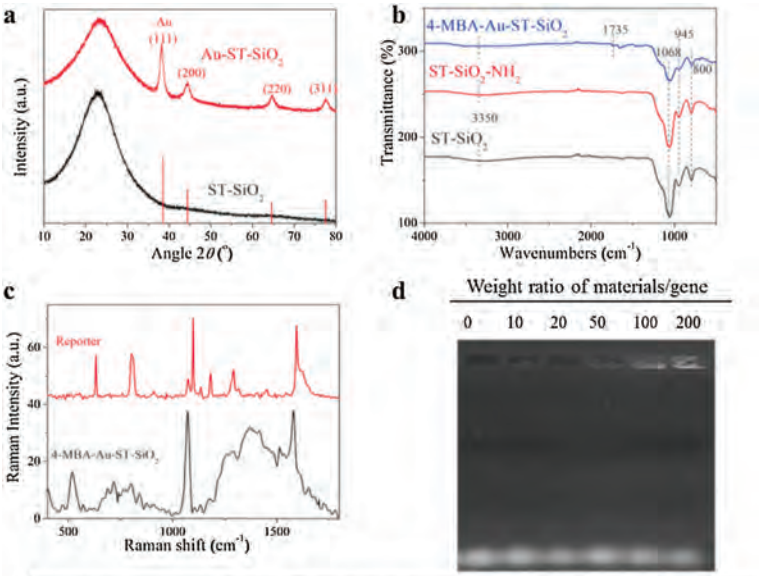

Name	Raman shift (cm^{-1})	Intensity (a.u.)	EEF
Reporter	1099.1	27.6	NA
4-MBA-Au-ST-SiO_2	1073.33	37.32	1.35×10^5

Fig. 2. (a) XRD parttern of Au-ST-SiO_2 and ST-SiO_2 with standard gold intensity obtained from JCPDS card No. 04-0784. (b) FTIR of 4-MBA-Au-ST-SiO_2, ST-SiO_2-NH_2 and ST-SiO_2. (c) Raman spectra of 4-MBA and 4-MBA-Au-ST-SiO_2. (d) Agarose gel retardation assay of 4-MBA-Au-ST-SiO_2/siRNA at different weight ratios. Table summarizes the Raman signal situation.

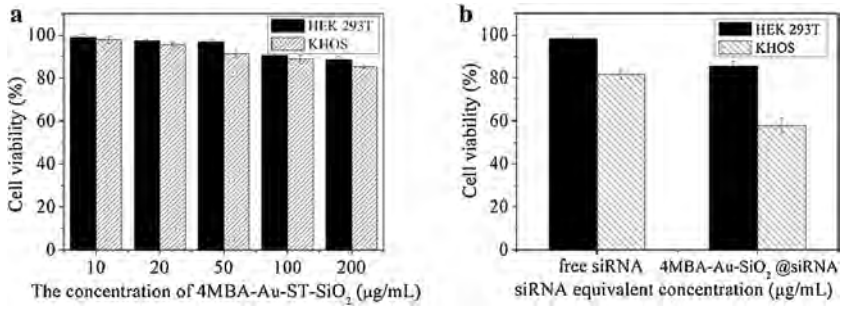

Fig. 3. (a) The biocompatibility and (b) cytotoxicity studies in healthy human cell line HEK 293T and human osteosarcoma cell line KHOS.

293T and KHOS cells remain above 85% with 4-MBA-Au-ST-SiO_2 nanocarriers concentration increase from 10 μg/mL to 200 μg/mL. Thus, 4-MBA-Au-ST-SiO_2 nanocarrier is biocompatible in both healthy and cancer cells, which means that the SERS tag design is non-destructive. The cytotoxicity of an equivalent concentration of 1 μg/mL free siRNA/cell growth medium and 200 μg/mL 4-MBA-Au-ST-SiO_2@siRNA/medium mixtures was testd by MTT assays. Note that 4-MBA-Au-ST-SiO_2@siRNA were fabricated based on the 200 wt ratio of 4-MBA-Au-ST-SiO_2 to siRNA. As demonstrated in Fig. 3b, free siRNA and 4-MBA-Au-ST-SiO_2@siRNA have little cytotoxicity in HEK 293T cells with cell viabilities around 98.2% and 85.7%. However, the results in KHOS cells have obvious difference. 1 μg/mL free siRNA is a bit cytotoxic in KHOS cells with 81.6% cell viability, while 4-MBA-Au-ST-SiO_2@siRNA with equivalent siRNA concentration demonstrates higher anti-cancer ability with corresponding cell viability of 57.7%. In consequence, 4-MBA-Au-ST-SiO_2 delivery system could load siRNA and delivery it into cells for siRNA therapy, suggesting that the loading of siNRA on 4-MBA-Au-ST-SiO_2 may inhibit its nuclease degradation to a certain extent due to the protection role of porous carriers [39–41].

Cellular uptake of 4-MBA-Au-ST-SiO_2 was observed with confocal Raman laser scanning microscopy. The traced SERS mapping images were taken based on the intensity of SERS peaks centred at Raman shift of 1073.3 cm^{-1}. Fig. 4a shows the optical image of KHOS cells containing 4-MBA-Au-ST-SiO_2. The mapping area with approximate 6 cells is shown by red rectangle frame, which is enlarged in the upper right corner with many tested points indicated by green cursors. The cell morphologies are as good as well-grown cells, which means they are healthy and alive at the moment of taking photos. The selected point 1 represents the signal obtained from the cell, while point 2 is that from the background substance (Fig. 4b). Their corresponding Raman spectra are demonstrated in Fig. 4c. The original mapping data are shown in Figs. S3 and S4 (Supporting information). The 1260 cm^{-1} peak is attributed to quartz substrates. The SERS peak centred at 1073.3 cm^{-1} at point 1 can be obviously noticed in Fig. 4c. The SERS mapping image in Fig. 4d shows that the brightness of red color reflects the intensity of 1073.3 cm^{-1} SERS peak with the value ranging from 10 to 70 (Figs. S3 and S4). Fig. 4e is the merged image, which shows that the SERS mapping image

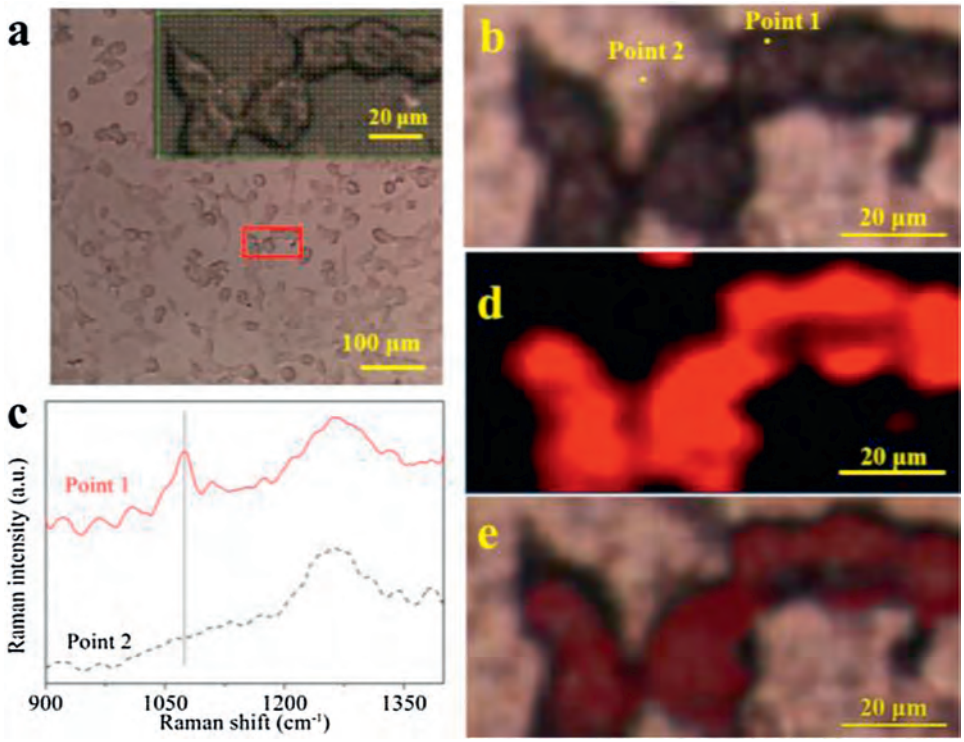

Fig. 4. (a) Optical image with marked selected mapping area; the inset shown the enlarged mapping area with each tested point. (b) Optical image with two selected points. (c) SERS spectra of points 1 and 2. (d) SERS image and (e) the merged image.

and optical image can match very well. This performance can confirm the feasibility of SERS tracing by using 4-MBA-Au-ST-SiO_2 as a tag. As the low quantity of 4-MBA is used in the cell and the cells are of healthy morphologies, the synthesized 4-MBA-Au-ST-SiO_2 gene delivery system has high sensitivity of SERS trace and non-destructive for cells.

The novel 4-MBA-Au-ST-SiO_2 SERS traceable delivery system has been synthesized by using a stellate porous silica as a platform. Many small Au nanoparticles were aggregated on silica skeleton by electrostatic interaction and capillary adsorption. The special Au@silica structure can endow the gene delivery system with SERS active effect. The 4-MBA-Au-ST-SiO_2 is biocompatible in both healthy HEK 293 and cancer KHOS cells. In contrast, 4-MBA-Au-ST-SiO_2@siRNA has higher anti-cancer ability with 57.7% cell viability against KHOS cells, while it has little cytotoxicity in HEK 293 cells with 85.7% of cell viability. Moreover, the developed 4-MBA-Au-ST-SiO_2 gene delivery system shows high sensitivity and non-invasive features of SERS trace. These results indicate the constructed 4-MBA-Au-ST-SiO_2@siRNA delivery system may be an alternative economic SERS tag applied in gene delivery system to replace conventional pure metallic ones.

Declaration of competing interest

The authors declare that they have no known competing financial interests or personal relationships that could have appeared to influence the work reported in this paper.

Acknowledgments

This work was financially supported by the Australian Research Council (ARC) Discovery Projects (Nos. DP140104062 and DP160104866). Fundamental Research Funds for the Central Universities (Nos. FRF-TP-19-017B1, 2302015-06500017, FRF-BR-19-003B, FRF-BD-20-14A) and National Natural Science Foundation of China (No. 21501009). Lei Liu acknowledged a scholarship from the University of Adelaide.

Appendix A. Supplementary data

Supplementary material related to this article can be found, in the online version, at doi:https://doi.org/10.1016/j.cclet.2020.12.061.

References

[1] D. Peer, J. Karp, S. Hong, et al., Nat. Nanotechnol. 2 (2007) 751–760.
[2] Y. Wang, P. Jarreau, Y. Xia, Nat. Mater. 10 (2011) 482–483.
[3] M. Davis, Z. Chen, D. Shin, et al., Nat. Rev. Drug Discovery 7 (2008) 771–782.
[4] Y. Wang, X. Du, Z. Liu, S. Shi, H. Lv, J. Mater. Chem. A: Mater. Energy Sustain. 7 (2019) 5111–5152.
[5] X. Du, S.Z. Qiao, Small 11 (2014) 392–413.
[6] H. Su, Q. Tian, C.A. Hurd Price, et al., Nano Today 31 (2020) 100834.
[7] L. Yin, Q. Tian, Y. Boyjoo, et al., Langmuir 36 (2020) 6984–6993.
[8] J. Liu, T. Liu, J. Pan, S. Liu, G.Q. Lu, Annu. Rev. Chem. Biomol. Eng. 9 (2018) 389–411.
[9] Z. Wang, G. Liu, H. Zheng, X. Chen, Biotechnol. Adv. 32 (2014) 831–843.
[10] Q. He, J. Shi, Adv. Mater. 26 (2014) 391–411.
[11] Y. Gao, J. Xie, H. Chen, et al., Biotechnol. Adv. 32 (2014) 761–777.
[12] C. Argyo, V. Weiss, C. Bräuchle, T. Bein, Chem. Mater. 26 (2014) 435–451.
[13] Z. Teng, X. Su, Y. Zheng, et al., Chem. Mater. 25 (2013) 98–105.
[14] X. Fang, X. Zhao, W. Fang, C. Chen, N. Zheng, Nanoscale 5 (2013) 2205–2218.
[15] M. Vendrell, K.K. Maiti, K. Dhaliwal, Y.T. Chang, Trends Biotechnol. 31 (2013) 249–257.
[16] B. Fahrenkrog, U. Aebi, Nat. Rev. Mol. Cell Biol. 4 (2003) 757–766.
[17] S. Keren, C. Zavaleta, Z. Cheng, et al., Proc. Natl. Acad. Sci. U. S. A. 105 (2008) 5844–5849.
[18] K.A. Stoerzinger, J.Y. Lin, T.W. Odom, Chem. Sci. 2 (2011) 1435–1439.
[19] S. Zong, Z. Wang, H. Chen, et al., IEEE Trans. Nanotechnol. 13 (2014) 55–60.
[20] S. Zong, Z. Wang, H. Chen, J. Yang, Y. Cui, Anal. Chem. 85 (2013) 2223–2230.
[21] D. Lin, T. Qin, Y. Wang, X. Sun, L. Chen, ACS Appl. Mater. Interfaces 6 (2014) 1320–1329.
[22] L. Xiao, S. Harihar, D.R. Welch, A. Zhou, Anal. Chim. Acta 843 (2014) 73–82.
[23] Z. Wang, S. Zong, W. Li, et al., J. Am. Chem. Soc. 134 (2012) 2993–3000.
[24] J. Xie, Q. Zhang, J.Y. Lee, D.I.C. Wang, ACS Nano 2 (2008) 2473–2480.
[25] J. Fang, S. Du, S. Lebedkin, et al., Nano Lett. 10 (2010) 5006–5013.
[26] Z. Wang, J. Zhang, J.M. Ekman, P.J.A. Kenis, Y. Lu, Nano Lett. 10 (2010) 1886–1891.
[27] Q. Li, Y. Jiang, R. Han, et al., Small 9 (2013) 927–932.
[28] Y. Lai, L. Dong, R. Liu, et al., Chin. Chem. Lett. 31 (2020) 2437–2441.
[29] A.M. Fales, H. Yuan, T. Vo-Dinh, Langmuir 27 (2011) 12186–12190.
[30] A.M. Fales, H. Yuan, T. Vo-Dinh, J. Mol. Pharm. Org. Process Res. 10 (2013) 2291–2298.
[31] H. Yuan, A.M. Fales, C.G. Khoury, J. Liu, T. VoDinh, J. Raman Spectrosc. 44 (2013) 234–239.
[32] J. Yang, L. Xia, Z. Lin, et al., Chin. Chem. Lett. 30 (2019) 638–642.
[33] L. Xiong, X. Du, B. Shi, et al., J. Mater. Chem. B: Mater. Biol. Med. 3 (2015) 1712–1721.
[34] K. Zhang, L.L. Xu, J.G. Jiang, et al., J. Am. Chem. Soc. 135 (2013) 2427–2430.
[35] X. Du, J. He, Nanoscale 4 (2012) 852–859.
[36] L. Wei, B. Jin, S. Dai, J. Phys. Chem. C 116 (2012) 17174–17181.
[37] A. Michota, J. Bukowska, J. Raman Spectrosc. 34 (2003) 21–25.
[38] P.H.C. Camargo, L. Au, M. Rycenga, W. Li, Y. Xia, Chem. Phys. Lett. 484 (2010) 304–308.
[39] W. Ngamcherdtrakul, J. Morry, S. Gu, et al., Adv. Funct. Mater. 25 (2015) 2646–2659.
[40] J. Morry, W. Ngamcherdtrakul, S. Gu, et al., Biomaterials 66 (2015) 41–52.
[41] M.Y. HanafiBojd, L. Ansar, B. Malaekeh-Nikouei, Ther. Deliv. 7 (2016) 649–655.